OPTIMAL MATCHING OF A SELF-EXCITED INDUCTION GENERATOR TO A SMALL WIND TURBINE

N. J. Batt and C. E. Coates

The University of Newcastle, Newcastle (Australia)

1. Introduction

The majority of small (< 50kW) wind turbines utilize permanent magnet (PM) generators [Wood, 2011]. These machines offer advantages that include relatively simple control and the ability to directly connect to the rotor without a gearbox. To achieve direct-drive, the PM generators are built in a multi-pole configuration that significantly increases the complexity, weight and price of the machine.

The self-excited induction generators (SEIG) are the simplest mechanically and usually the cheapest form of generator [Eggleston and Forrest, 1987], but are traditionally considered to have a limited range of speed. In this paper, the SEIG is examined using steady state and dynamic modeling in Matlab / Simulink. These models are combined with the mechanical power curve of a 5kW wind turbine to optimize the SEIG and self-excitation capacitance selection for a particular wind turbine. The paper shows the theoretical power curve achievable with the chosen generator and rotor combination. This is important as frequently wind turbines are characterized by their mechanical characteristic and the limitations imposed by the generator are ignored.

A dynamic model of the SEIG was created using the 'Ideal Rotating Transformer' (IRTF) concept [Veltman et al., 2007]. This model was expanded to include saturation in the machine's magnetizing inductance and self-excitation capacitance. The SEIG is simulated supplying power into a resistive load.

Simulated results are verified against experimental results obtained from a 4-pole, nominally 3kW induction motor which has been used for prototype testing of the Aerogenesis 5kW wind turbine. In order to create an accurate model, it was necessary to perform an enhanced version of standard machine characterization tests. Enhancements include assessing the effect of heating, as well as measuring the saturation curve – magnetizing inductance vs. phase voltage – for various stator voltage frequencies.

The steady state and dynamic models were assessed against the designed maximum power point curve of a 5kW wind turbine to see how well they match. The excitation capacitance was varied to find the optimum value for the particular generator/turbine combination.

1.1 List of Symbols Used

Power Coefficient	C_P	Magnetising Inductance (H)	L_M
Stator Resistance (Ω)	R_S	Rotor Resistance (Ω)	R_R
Leakage Inductance (H)	L_σ	Electrical Slip	s
Electrical angular frequency (rad/s)	ω_S	Rotor EMF (V)	e_M
Mechanical angular frequency (rad/s)	ω_M	Total Reactive Power (VAR)	Q_t
Magnetising flux linkage (Wb)	ψ_M	Load Resistance (Ω)	R_L
Excitation Capacitance (F)	C_E	Imaginary Component	$\mathfrak{I}$
Stator Phase Current (A)	I_S	Tip Speed Ratio	TSR

2. Wind Turbine Power Curve

Tip Speed Ratio refers to the ratio between the circumferential velocity of the blade tips and the wind speed [Wood, 2011]. TSR has a strong impact on the ratio of extracted power vs the power available in the wind, known as the power coefficient. Figure 1 demonstrates this relationship on a generic 5kW turbine [Riawan

and Nayar, 2009].

Tip speed ratios from 7 to 11 are considered the optimum range for maximum power extraction from the Aerogenesis Turbine. It can be seen that for a particular wind speed, the output power does not vary considerably in this range. Once outside this range, output power drops off significantly as C_P reduces.

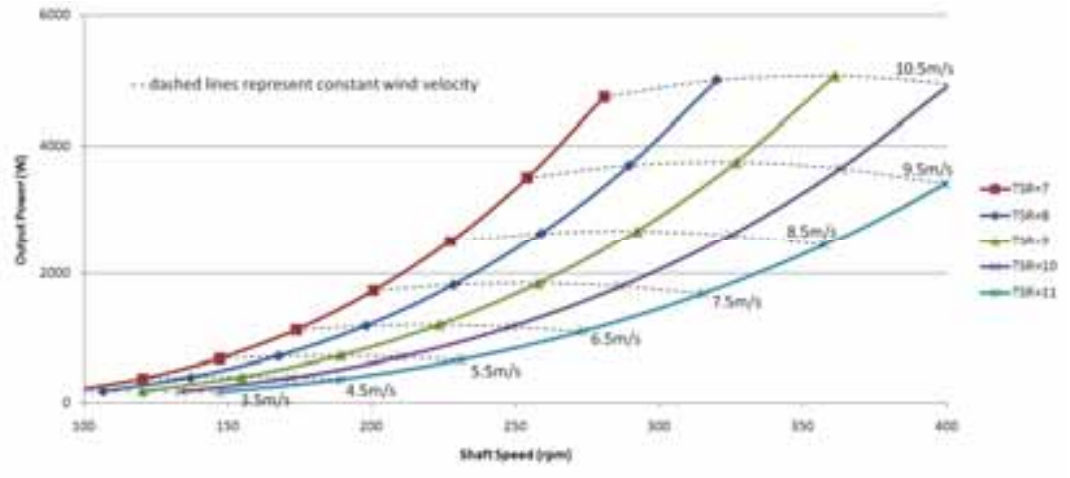

Fig. 1: Output power vs shaft speed for varying TSR and wind speeds

3. Generator Power Curve

In order to produce a generator power curve for a SEIG, good knowledge of machine parameters is needed and an optimum level of excitation capacitance must be chosen. For this paper, a combination of empirical testing, steady state analysis and dynamic analysis was used to develop a comprehensive power curve that takes into account multiple factors including magnetic saturation and heating effects.

3.1. Parameter Identification

For a SEIG, there is no external voltage supply and the output voltage is produced through residual flux exciting a resonance between the excitation capacitors and magnetizing inductance. Changes in machine parameters, especially magnetizing inductance, due to saturation and heating effects will generate large errors in the model if not taken into account. In fact it is saturation that provides the negative feedback, controlling resonance and hence output voltage to safe levels.

Figure 2 shows a two-inductor model of an Induction Machine. This differs from the standard three-inductor model; however it can be shown that the entire machine dynamics as seen from the stator terminals can be accurately modeled [Veltman et al., 2007]. Reducing the model to two inductors greatly simplifies analysis and also makes it easier to identify machine parameters.

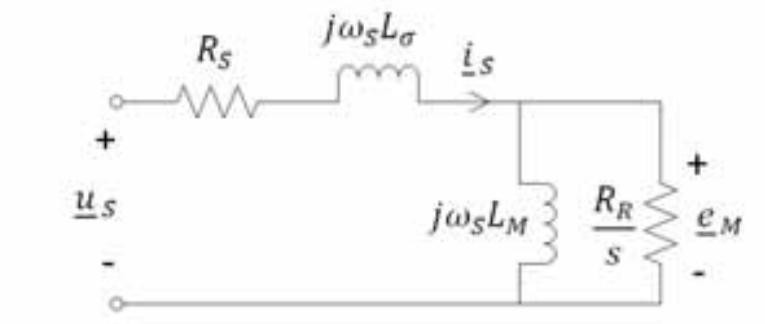

Fig. 2: Induction machine two-inductor steady-state model L_sigma is not in the symbol list

A 3kW Donly induction machine, with nameplate data included in Appendix A, was analysed to identify machine parameters. Traditional induction machine parameter identification involves Blocked Rotor and No

Load tests [Sarma and Pathak, 2010].

The Blocked Rotor test is usually carried out at rated current and frequency. Due to the required accuracy for the SEIG model, this test was carried out at various levels of current, frequency and heat. Leakage inductance displayed variation due to these factors, but this was found not to affect accuracy significantly in the frequency range where the majority of power is produced. The average leakage inductance level was found to be 16.8mH.

Rotor and stator resistance R_S and R_R were found to vary significantly with heat as shown in Table 1.

Tab. 1: Measurements of Rotor and Stator Resistance with varying temperature

	Measured at room temp 25ºC. Referred to as 'cold'	**After 30 mins running hot. Approximate winding temperature 90ºC**
Stator Resistance R_S	2.1Ω	2.7Ω
Rotor Resistance R_R	1.4Ω	1.9Ω

No load tests are usually carried out at rated voltage and frequency. The saturation curve of an induction machine is of fundamental importance to a SEIG, so measurements need to be taken at various voltage levels.

Magnetising Inductance defines the relationship between flux-linkage and current in *linear* magnetic circuits [Veltman et al., 2007] according to equation 1. When saturation is evident, this relationship is no longer linear and the *L* term becomes variable with respect to current.

$$\psi_M = Li \quad \text{(eq. 1)}$$

Flux linkage can be calculated from no load measurements according to equation 2, in RMS form.

$$\Psi_M = \frac{Q_c}{\omega_S I_S} - I_S L_\sigma \quad \text{(eq. 2)}$$

The no load test was carried out with varying voltages and frequency. The results of this test can be seen in Figure 4. It is clear that frequency of supply does not significantly affect the relationship between flux-linkage and current in the range of 20Hz to 70Hz. A 6th order polynomial fit using the 50Hz data was found to accurately reflect this relationship.

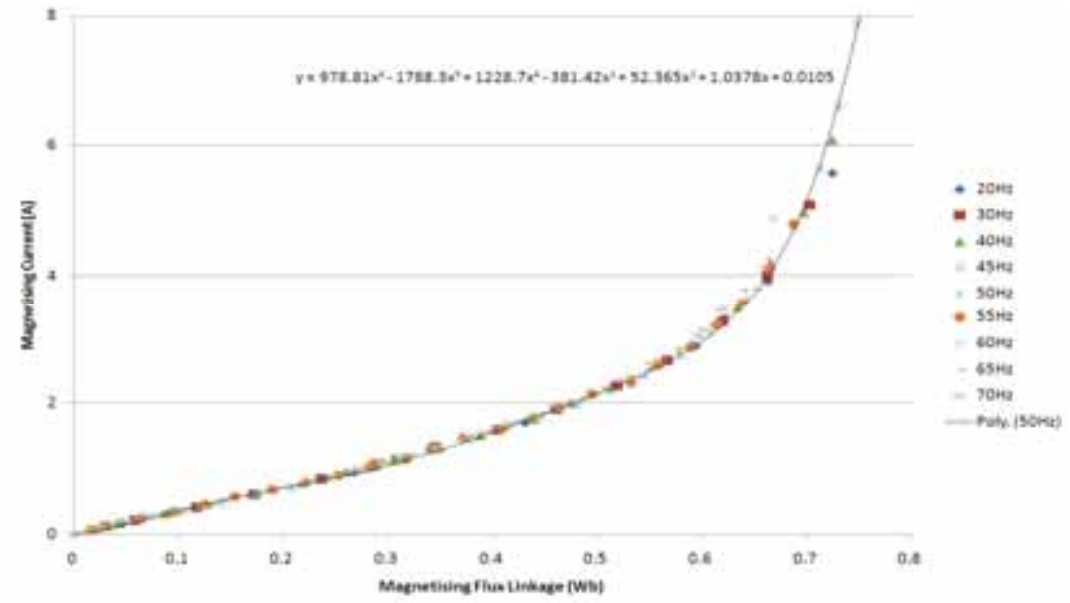

Fig. 3: Relationship between magnetizing current and flux-linkage as the induction machine saturates.

3.2. *Empirical Testing*

It is well known that connecting capacitors across stator terminals will allow an induction machine to self-excite [Arrilaga and Watson, 1978] and that the amount of capacitance determines the speed range for which this will occur. The 3kW Donly gearmotor had 3 star-connected capacitors connected in parallel to the load. Assuming a balanced system, the steady-state equivalent circuit is shown in Figure 4.

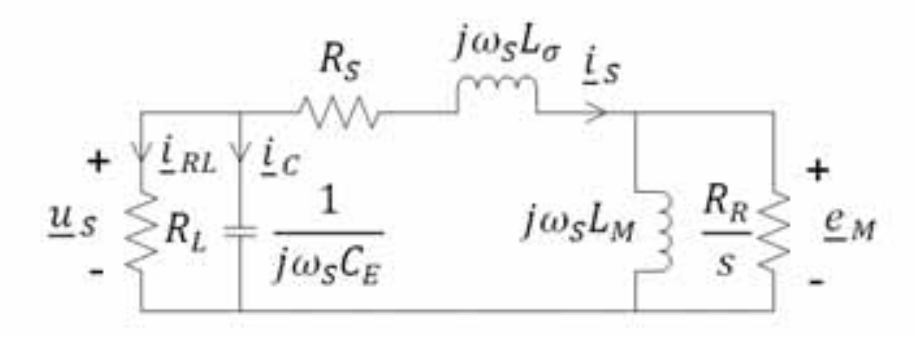

Fig. 4: Steady-state two-inductor equivalent circuit of a Self-Excited Induction Generator

Tests were carried out with capacitances of 50µF, 75µF and 100µF per phase. For a given capacitance, the machine was driven by an external prime mover until the SEIG was observed to self-excite. At this point, a resistive load was added and varied until a maximum power point was found. The speed was then increased and a maximum power point was found for various speeds. The results of this test can be seen in Figure 5.

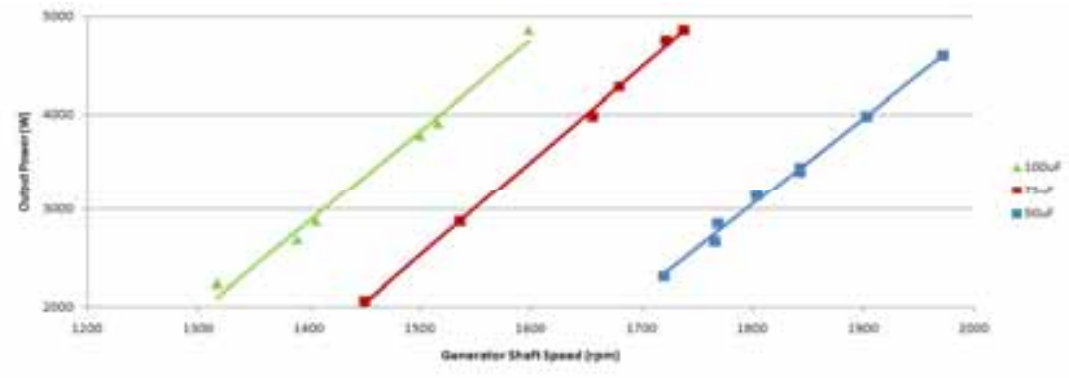

Fig. 5: Maximum power curves of SEIG with various levels of excitation capacitance.

Since the synchronous speed of the generator is 1500 rpm, it was decided that the midpoint of the power curve should be around this value. 70µF was chosen based on the comparison in Figure 5 for excitation capacitance. It has the effect of moving the maximum power point slightly to the right compared with 75µF. A more comprehensive maximum power point curve was produced for the 70µF excitation as shown in Figure 6.

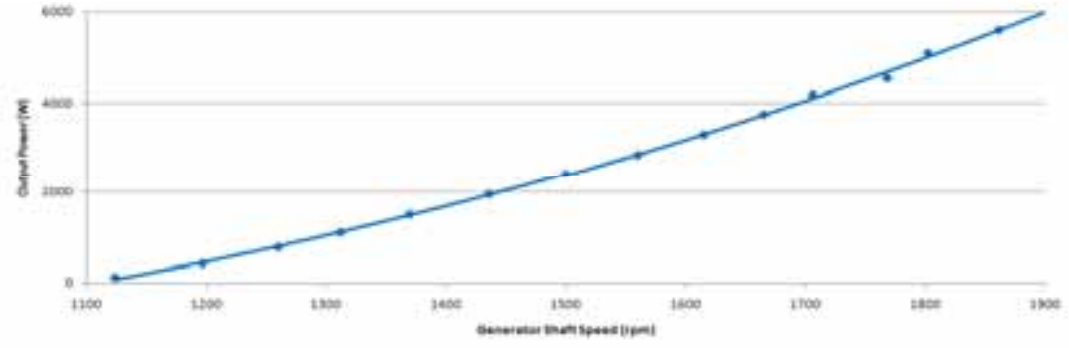

Fig. 6: Measured maximum power point of SEIG with 70µF excitation capacitance per phase

3.3 Dynamic Analysis

A dynamic model was developed based on the Ideal Rotating Transformer (IRTF) concept introduced by Veltman et al [2007]. In the book, the input was normally a voltage or flux-linkage space vector. For the SEIG, these variables are outputs. The sole input into the SEIG model is shaft speed. Considering this fundamental difference, some important modifications had to be made.

The overview diagram of the dynamic simulation is shown in Figure 7. The central component of this simulation is the induction generator. The Excitation and Load module provides a feedback loop as in the real SEIG, which controls output voltage and current. This allows the simulation to have a single input, shaft speed.

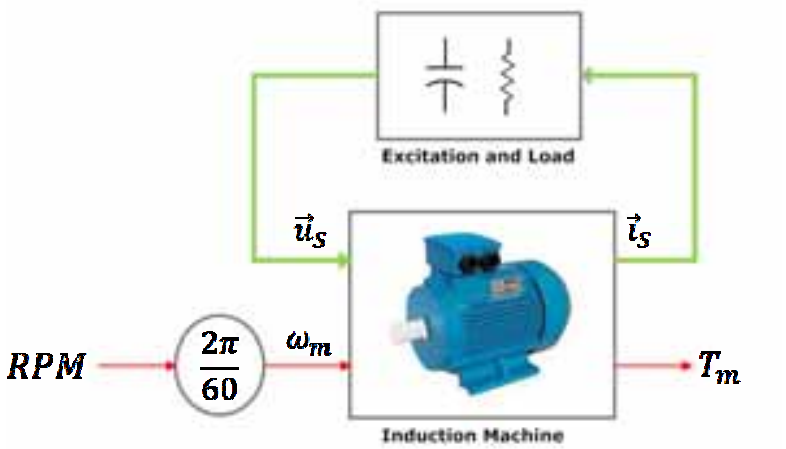

Fig. 7: Dynamic Simulation

This model is intended to be connected to a dynamic simulation of a wind turbine's mechanical system, which will use the calculated torque as feedback and provide shaft speed to the model. In this paper, focus is on assessing the steady state accuracy of the SEIG model and so input frequency will be maintained at a constant level.

The Excitation and Load module is shown in Figure 8, which is a dynamic model of a parallel RC load.

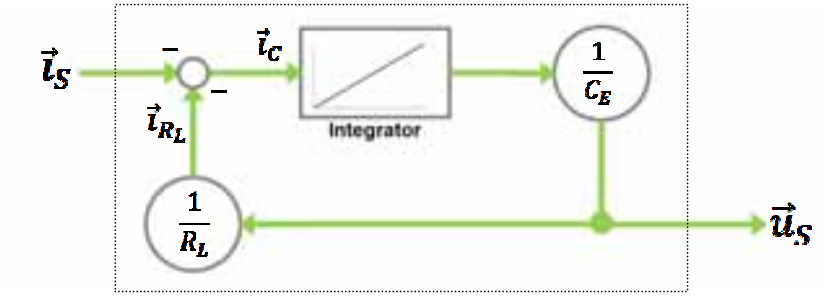

Fig. 8: Excitation and load

Figure 9 shows the Induction Generator sub-circuit of the dynamic simulation. The primary modification made for this paper is the replacement of the $^{1}/_{L_M}$ gain block between rotor flux linkage and magnetizing current with the non-linear function from Figure 3. The integrator module that converts $\vec{e}_M^{xy}$ to $\vec{\psi}_M^{xy}$ has been configured with a nonzero initial condition $\vec{\psi}_M^{xy}(0) = 0.1Wb$ to simulate remnant flux.

The simulation is based around an "IRTF Current" module, which translates signals between the "αβ" stator frame and the "xy" rotor frame. It also calculates torque in the machine using equation 3. There is a factor of 2 when converting angles and torque between mechanical and electrical values because there are two pairs of windings in a 4-pole motor [Veltman et al., 2007].

$$T_e = \Im\{\vec{\psi}_M \vec{\imath}_S\} \quad \text{(eq. 3)}$$

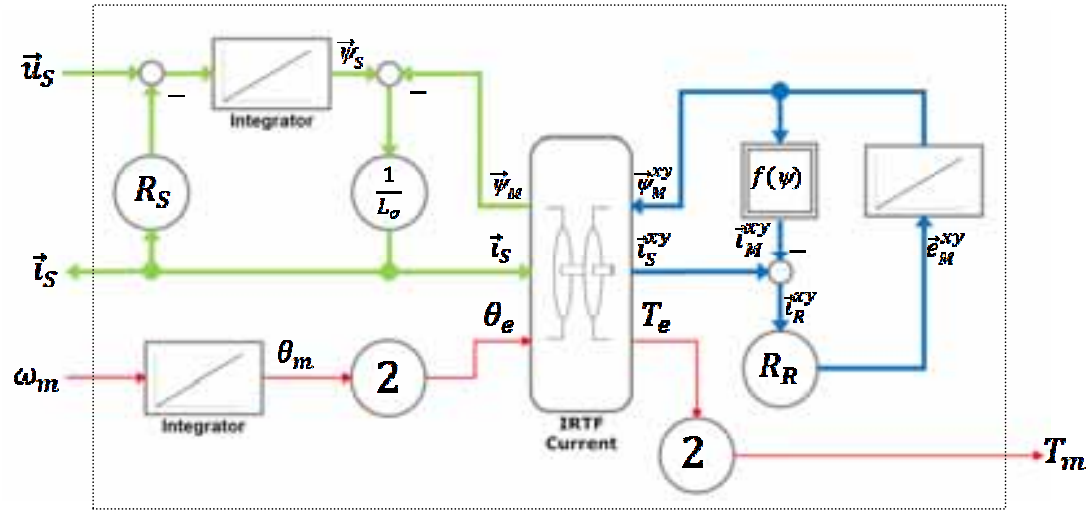

Fig. 9: Induction Machine Simulation including saturation effects.

Magnetic saturation is modeled in Figure 9 using the non-linear formula $f(\psi)$. Figure 4 shows per-phase steady state values. Because of this, $\vec{\psi}_M^{xy}$ is converted to RMS form $\psi_M = \frac{1}{\sqrt{3}}|\vec{\psi}_M^{xy}|$. The per-phase RMS value of the magnetizing current is then calculated using the 6th order polynomial best fit from Figure 3. The result is converted back into space vector form, where $|\vec{i}_M^{xy}| = \sqrt{3} I_M$ and $\angle\vec{i}_M^{xy} = \angle\vec{\psi}_M^{xy}$.

The configuration parameters of excitation capacitance, load resistance and shaft speed that led to the maximum power point graph of Figure 6 were fed into the dynamic model. Both hot and cold resistance values were used with the results as shown in Figure 10. It can be seen that the measured results resemble cold simulation at low power and hot simulation at high power. This is expected, since the machine will heat up quickly at high power levels.

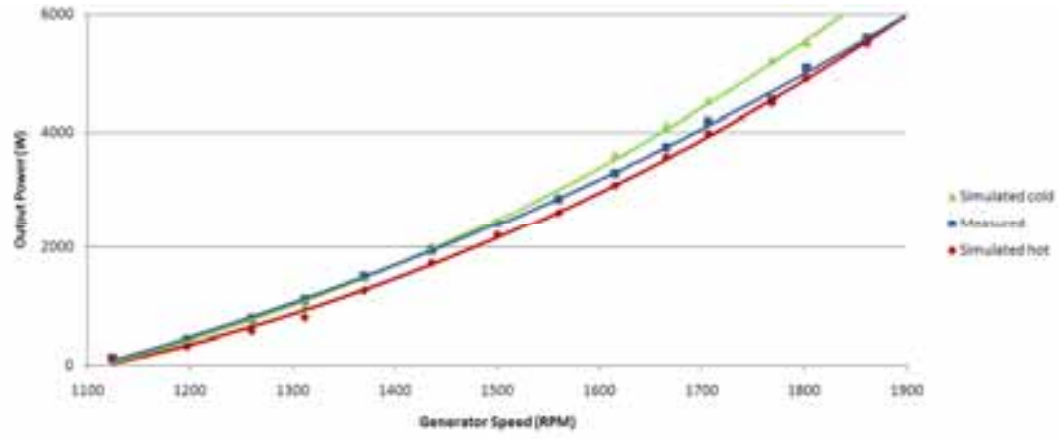

Fig. 10: Dynamic simulation results for hot and cold resistance values, compared to measured results from Figure 7

As shown in Figure 10, the results of the dynamic simulation closely resemble measured results. This model was based on measurements described in section 3.1 and shows that the dynamic model represents the SEIG accurately. The benefits of using a simulation model is that a lot of development work can be carried out without running the electric machine. It also allows insights into how the SEIG operates and makes a good base for simulating the whole turbine.

3.4 Steady State Calculations

Steady-state calculations allow many scenarios to be tested quickly by using small incremental steps. This makes it much more efficient than empirical testing and dynamic modelling to build power curves if knowledge of the dynamic response is not required.

From Figure 4, summing currents at the load.

$$\underline{i_S} = \underline{u_S}(-R_L^{-1} - j\omega_S C_E) \quad \text{(eq. 5)}$$

From Figure 4, the generator voltage current relationship is [Veltman et al., 2007].

$$\underline{i_S} = \frac{\underline{u_S}(R_R/s + j\omega_S L_M)}{j\omega_S L_M R_R/s + (R_S + j\omega_S L_\sigma)(R_R/s + j\omega_S L_M)} \quad \text{(eq. 6)}$$

Combining Equation 5 with Equation 6

$$-R_L^{-1} - j\omega_S C_E = \frac{R_R/s + j\omega_S L_M}{j\omega_S L_M R_R/s + (R_S + j\omega_S L_\sigma)(R_R/s + j\omega_S L_M)} \quad \text{(eq. 7)}$$

Expanding and equating real parts gives the following expression for slip

$$s = \left(\frac{R_R}{\omega_S^2 L_M}\right)\left(\frac{R_L + R_S - C_E R_L \omega_S^2 (L_M + L_\sigma)}{L_\sigma + C_E R_S R_L}\right) \quad \text{(eq. 8)}$$

Equating imaginary parts and using simultaneous equations arrives at the following expression for magnetizing inductance, which depicts the point where saturation of L_M balances the LC resonant effect;

$$L_M = \frac{\left(C_E R_S + \frac{L_\sigma}{R_L}\right)^2 + \left(\frac{R_L + R_S}{R_L \omega_S} - C_E L_\sigma \omega_S\right)^2}{C_E - C_E^2 \omega_S^2 L_\sigma - L_\sigma / R_L^2} \quad \text{(eq. 9)}$$

There are two unknowns in Equation 9, L_M and ω_S. Since slip is relatively small, we can initially assume slip=0, making $\omega_s = \frac{\omega_m}{1-s} = \omega_m$. Once a value for L_M is found, this result can be fed back into Equation 8 to approximate a value for slip. This would then be fed back into Equation 9 to find a more accurate value for L_M. This process can continue until the desired level of accuracy is achieved. Three iterations have been found sufficient.

Using the same data as Figure 3, the steady state magnetising inductance for varying magnetising current values was found as shown in Figure 11. This is related to the slope of the flux-linkage vs current curve and is effectively a steady-state linearization.

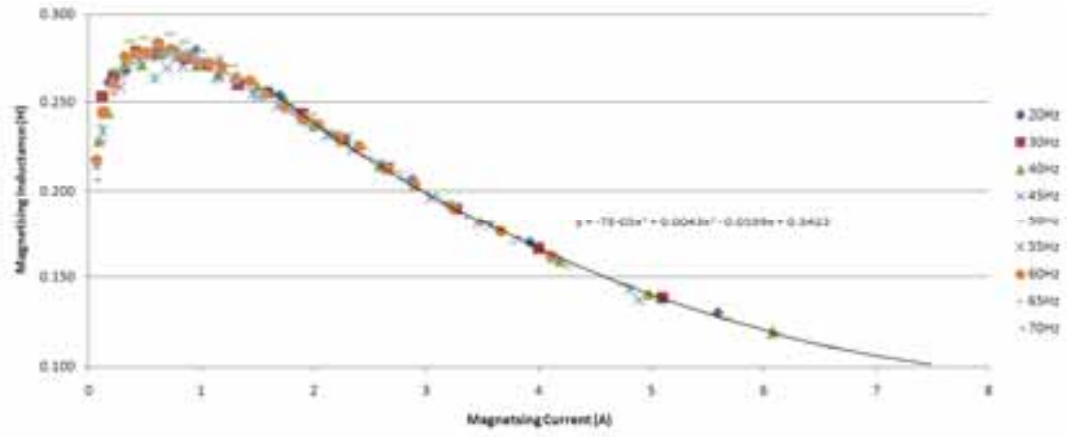

Fig. 11: Steady-state measurements of magnetising inductance with increasing magnetising current

It can be seen that when magnetising current is below 1.5A, there is significant variance in magnetising inductance for different frequency inputs. This is due to small measurement errors, amplified by the linearization process. As such, the steady state model will not be accurate at low currents. In practise, we are interested in the regions where exploitable power is produced, so setting 1.5A as the minimum current is not a significant issue.

The trend line on Figure 11 is a 3rd order polynomial best fit based on data where magnetising current is between 1.5A and 7.5A. Inverting the best-fit equation produces the formula shown in Equation 10.

$$I_M = -1372L_M^3 + 886.9L_M^2 - 215.1L_M + 21.5 \quad \text{(eq. 10)}$$

By defining $\underline{i}_M \triangleq \sqrt{3} I_M$ we can then calculate all significant variables using the following equation set [Veltman et al., 2007].

$$\underline{\psi}_M = L_M \underline{i}_M \quad \text{(eq. 11a)}$$

$$\underline{e}_M = j\omega_S \underline{\psi}_M \quad \text{(eq. 11b)}$$

$$\underline{e}_M^{xy} = j(\omega_S - \omega_m)\underline{\psi}_M \quad \text{(eq. 11c)}$$

$$\underline{i}_R = \frac{\underline{e}_M}{R_R/s} \quad \text{(eq. 11d)}$$

$$\underline{i}_S = \underline{i}_R + \underline{i}_M \quad \text{(eq. 11e)}$$

$$\underline{u}_S - \underline{e}_M = \underline{i}_S R_S + j\omega_S L_\sigma \underline{i}_S \quad \text{(eq. 11f)}$$

$$T_e = 3\left\{\underline{\psi}_M^* \underline{i}_S\right\} \quad \text{(eq. 11g)}$$

After performing the above calculations, output power of the steady state model was compared with the dynamic model as shown in Figure 12.

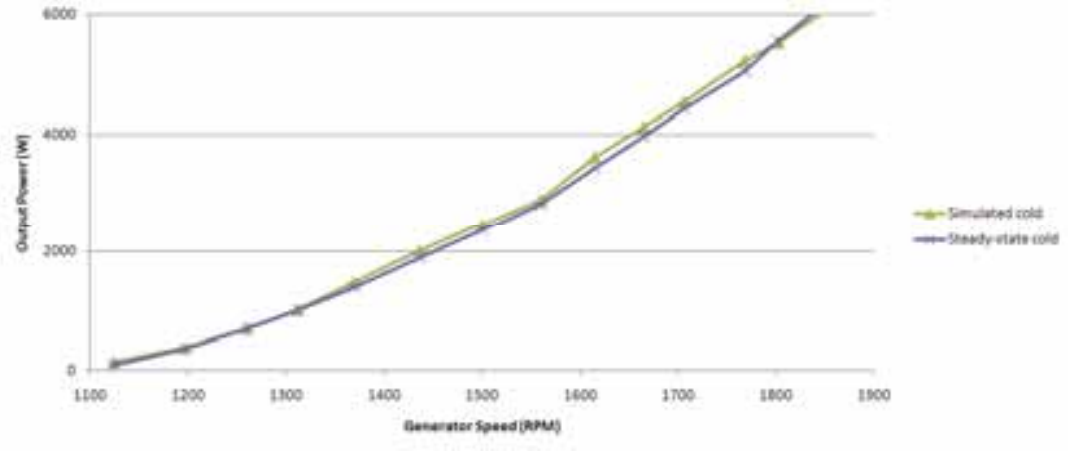

Fig. 12: Dynamic model compared to steady-state model

3.5 Calculating Range of Efficient Operation of Generator

In addition to the maximum power point, it is important to know the region of operation where the generator is most efficient. Figure 13 shows that the power curve for maximum efficiency lies slightly lower than the maximum power curve.

A third curve is introduced which shows the minimum power the generator can deliver, while retaining the efficiency of the maximum power curve. Below this point, efficiency of the generator is reduced significantly. The fourth curve of Figure 13 shows a power curve limited by maximum RMS phase voltage of 300V and a minimum phase current of 1.5A. 300V has been determined as the maximum safe working voltage of the SEIG.

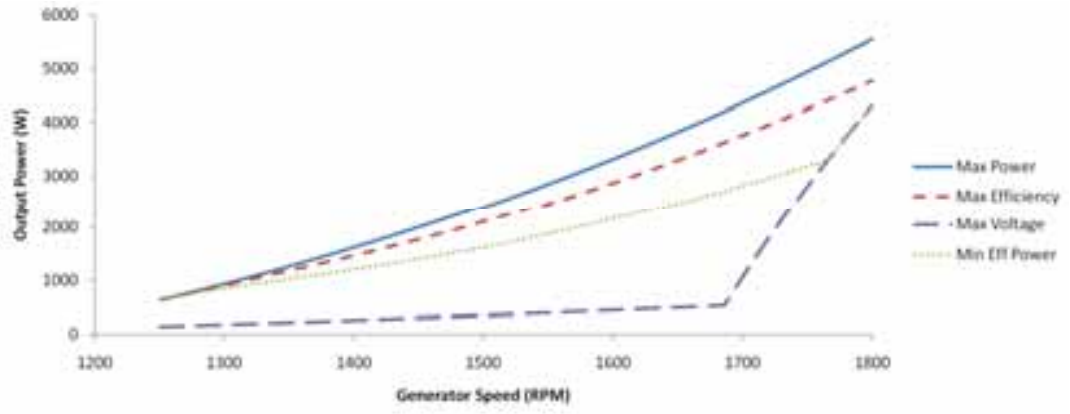

Fig. 13: Power Curves for various regions of operation of the SEIG

Figure 14 shows the efficiency of the SEIG for the various power curves shown in Figure 13. As expected, the minimum efficient power curve matches the efficiency of the maximum power curve in most speed ranges. The minimum power curve is realised by reducing output current and allowing phase voltage to increase. At around 1770RPM this is restricted by the maximum 300V phase voltage and the minimum power curve will follow the maximum voltage curve.

It should be noted that the trends in Figure 14 only consider electrical efficiency. The electrical machine test rig used to gather this data does not have an operational torque transducer that would allow the measurement of mechanical losses. Electrical efficiency has been verified in the model by summing output power and resistive losses from the stator. This has been found to match the product of torque and frequency which represents the theoretical mechanical power assuming no mechanical losses. Upgrades are planned for the test rig that will allow mechanical losses to be measured and included in the model.

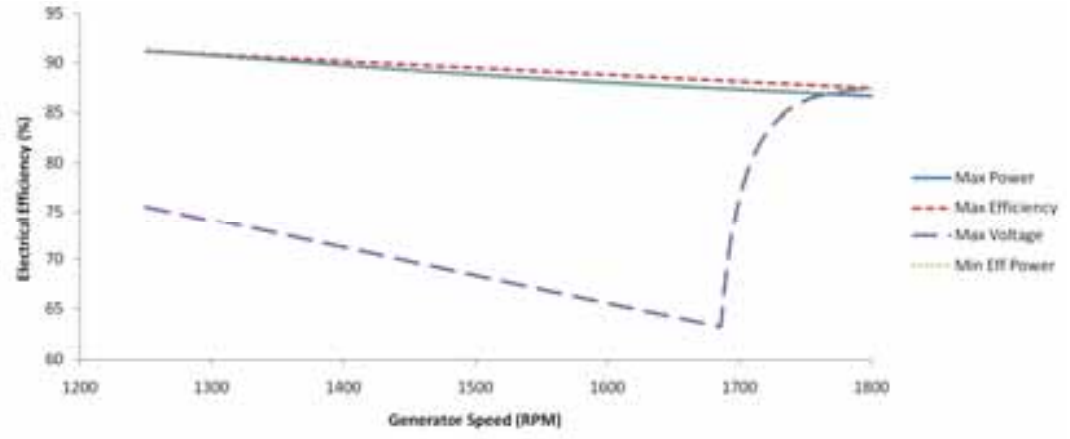

Fig. 14: Efficiency curves for various regions of operation of the SEIG

4. Matching Rotor and Generator Power Curves

In Figure 15, The Maximum Power Point (MPP) and Minimum Efficient Power (MEP) from Figure 13 have been overlaid on the power loci of the 5kW wind turbine from Figure 1. The wind turbine shaft speed has been multiplied by a factor of 8, to account for the 8:1 gearbox between the turbine shaft and the generator shaft.

Generally, it would be preferable for the efficient power region of the generator to match the maximum power range of the wind turbine. With the basic star-connected excitation capacitors of the SEIG studied in this paper this is not possible for the full region of operation. The capacitor selection of 70µF allows the power curve to remain within the optimal TSR range for winds ranging from 3.5m/s to 6.5m/s. This would be suitable for sites with low average wind speed.

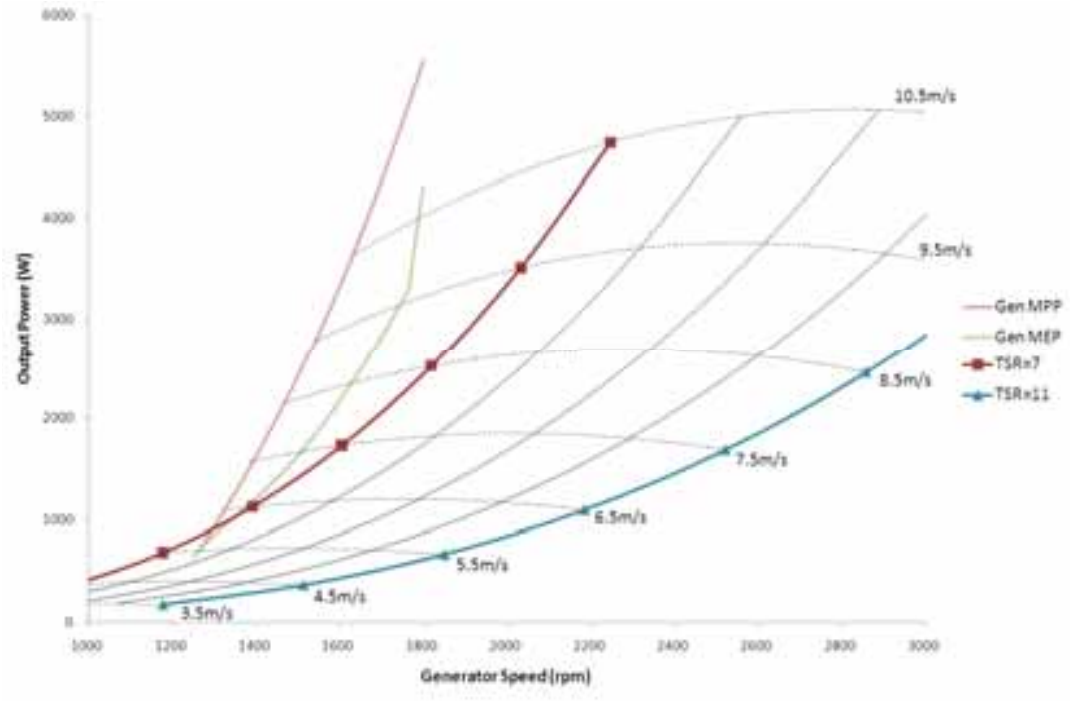

Fig. 15: Matching generator and wind turbine power curves

It can be seen in Figure 15 that as wind speed increases beyond 6.5m/s, the generator power curve moves further from the optimal TSR range. The maximum power curve of the generator may be controlled more precisely using controlled converters [Wang et al., 2008] or shunt-series capacitors [Riawan and Nayar, 2009]. It must be investigated further whether the extra complexity of these options will be outweighed by the improved power output.

5. Conclusion

The dynamic and steady state models described in this paper represent powerful tools for improving the performance and stability of SEIGs used in small wind turbines. When combined with an accurate wind turbine mechanical and aerodynamic model, the system can be optimized for maximum power extraction.

For optimum power extraction, focus should be on the power eventually delivered to the load. This should be calculated for all wind speeds. In Figure 15, a compromise was made to focus on power from low wind speeds. This was necessary because there is a relatively small speed range where the studied SEIG could operate and the prototype wind turbine was placed in a relatively low wind location. If smaller amounts of capacitance are used, the system can be optimized for higher wind speeds at the expense of low speed performance.

The models used for this paper will be extended in future work to assess alternative induction machines, different gearbox ratios and various configurations for self-excitation. This work will involve extensive use of simulations, followed by experimental validation in the lab and finally on the prototype wind turbine.

6. Acknowledgment

This work contributed to the development of the Aerogenesis 5 kW wind turbine with support from the Asia-Pacific Partnership for Clean Development administered by the Department of Energy, Resources, and Tourism.

7. References

Wood, D., 2011. Small Wind Turbines: Analysis, Design, and Application, Springer UK.

Eggleston, D., Forrest, S., 1987. Wind Turbine Engineering Design, Van Nostrand, New York.

Veltman, A., Pulle, D., De Doncker, R., 2007. Fundamentals of Electrical Drives, Springer Germany

Sarma, M., Mukesh, K., 2010. Electric Machines, Cengage Singapore

Arrillaga, J., Watson, D., 1978. Static Power Conversion from Self-excited Induction Generators. Proc. IEE, Vol. 123, No. 8.

Wang, L., Chen, H., Lee, D., 2008. Implementation of a DSP-Based Power Converter for a Wind Induction Generator. PES General Meeting.

Riawan, D., Nayar, C., 2009. Improved Power Transfer Capability of SEIG in Variable Speed Wind Turbine Generation System. AUPEC Proc.

Appendix A: 3kW DONLY INDUCTION MACHINE NAMEPLATE DATA

The 3kW induction machine used in this paper had the following nameplate data relevant for use as a motor:

Manufacturer	Donly
Power	3kW
Power Factor	0.82
Voltage L-L	380V
Current	6.8A
Frequency	50Hz
Insulation Class	F
Duty	1
Speed	1420 RPM